Multistep Photochemical Charge Separation in Rod-like Molecules Based on Aromatic Imides and Diimides

Scott R. Greenfield,[†] Walter A. Svec,[†] David Gosztola,[†] and Michael R. Wasielewski*[,†,‡]

Contribution from the Chemistry Division, Argonne National Laboratory, Argonne, Illinois 60439-4831, and Department of Chemistry, Northwestern University, Evanston, Illinois 60208-3113

Received January 10, 1996[⊗]

Abstract: A series of intramolecular triads with linear, rod-like structures has been developed that undergo very efficient two-step electron transfer following direct excitation of a chromophore possessing a charge transfer (CT) excited state. The CT state of 4-aminonaphthalene-1,8-imide (ANI), produced by direct excitation of the chromophore, has about 70% of a negative charge transferred from the amine to the imide. Attachment of aniline (An) and *p*-methoxyaniline (MeOAn) donors to ANI by means of a piperazine bridge results in linear dyads, **An-ANI** and **MeOAn-ANI**, that undergo rapid electron transfer in about 10^{-11} s to give a >99% yield of the ion pairs, **An**$^+$**-ANI**$^-$ and **MeOAn**$^+$**-ANI**$^-$, in which the charges are separated by 7.7 Å. The formation and decay of these ion pairs can be monitored directly by transient absorption spectroscopy. Further attachment of a 1,8:4,5-naphthalene-diimide (NI) electron acceptor to the imide group of ANI using a 2,5-dimethylphenyl spacer results in triads **An-ANI-NI** and **MeOAn-ANI-NI**. Excitation of the CT state of ANI within these triads results in the same high yield charge separation step observed in the corresponding dyads followed by a subnanosecond charge shift reaction to yield the giant dipole states **An**$^+$**-ANI-NI**$^-$ and **MeOAn**$^+$**-ANI-NI**$^-$ in 72% and 92% yield, respectively, in toluene. The lifetime of **MeOAn**$^+$**-ANI-NI**$^-$ is 310 ns. These triad molecules make explicit use of a CT excited state to initiate a multistep electron transfer process. The excited singlet CT state and the two ion pair states are all spectroscopically distinct, and all states are unambiguously spectrally resolved by transient absorption measurements. In addition, the ion pair states **An**$^+$**-ANI**$^-$ and **MeOAn**$^+$**-ANI**$^-$ undergo radiative recombination, thereby allowing a more detailed analysis of the energetics of charge separation and the influence of the CT excited state on the rates of subsequent longer distance charge shift reactions in these molecules.

Introduction

The reaction center proteins of photosynthetic organisms convert photon energy into chemical potential using an initial excited state electron transfer reaction followed by a sequence of dark electron transfers.[1−3] In recent years this same multistep electron transfer strategy has been used to synthesize and study a wide variety of electron donor−acceptor supermolecules designed to mimic key features of the primary photosynthetic charge separation.[4−6] Many of these model systems are based on chromophores that are related to the ones found in the photosynthetic reaction center, such as chlorophylls, porphyrins, and quinones. Chlorophylls and porphyrins are used most frequently as the chromophores that absorb light. Electron transfer from their lowest excited singlet or triplet states typically reduces a quinone electron acceptor. Secondary electron donors and/or acceptors further separate the charges within the initially formed radical ion pair by subsequent dark electron transfer reactions.[5,7−16] In one chlorophyll−porphyrin−quinone system a final radical ion pair lifetime of 8 ms with a 90% quantum yield of charge separation is achieved in a low temperature glass.[14]

While porphyrin-quinone-based multistep electron transfer systems have proven very successful for creating efficient long-lived charge separation, porphyrin cation and quinone anion radicals are often difficult to identify spectroscopically, which

[†] Argonne National Laboratory.
[‡] Northwestern University.
[⊗] Abstract published in *Advance ACS Abstracts,* June 15, 1996.

(1) Finkele, U.; Lauterwasser, C.; Struck, A.; Scheer, H.; Zinth, W. *Proc. Natl. Acad. Sci. U.S.A.* **1992**, *89*, 9514−9519.
(2) Diner, B. A.; Babcock, G. T. *Structure, dynamics, and energy conversion efficiency in Photosystem II.*; Diner, B. A., Babcock, G. T., Eds.; Kluwer: Dordrecht, 1996; pp 213−247.
(3) Heller, B. A.; Holten, D.; Kirmaier, C. *Science* **1995**, *269*, 940−945.
(4) Wasielewski, M. R. *Chem. Rev.* **1992**, *92*, 435−461.
(5) Gust, D.; Moore, T. A.; Moore, A. L. *Acc. Chem. Res.* **1993**, *26*, 198−205.
(6) Kurreck, H.; Huber, M. *Angew. Chem., Int. Ed. Engl.* **1995**, *34*, 849−866.
(7) Lee, S.-J.; DeGraziano, J. M.; Macpherson, A. N.; Shin, E.-J.; Kerrigan, P. K.; Seely, G. R.; Moore, A. L.; Moore, T. A.; Gust, D. *Chem. Phys.* **1993**, *176*, 321−336.
(8) Hung, S.-C.; Lin, S.; Macpherson, A. N.; DeGraziano, J. M.; Kerrigan, P. K.; Liddell, P. A.; Moore, A. L.; Moore, T. A.; Gust, D. *J. Photochem. Photobiol. A: Chem.* **1994**, *77*, 207−216.
(9) Gust, D.; Moore, T. A.; Moore, A. L.; Lee, S.-J.; Bittersmann, E.; Luttrull, D. K.; Rehms, A. A.; DeGraziano, J. M.; Ma, X. C.; Gao, F.; Belford, R. E.; Trier, T. T. *Science* **1990**, *248*, 199−201.
(10) Gust, D.; Moore, T. A.; Moore, A. L.; Macpherson, A. N.; Lopez, A.; DeGraziano, J. M.; Gouni, I.; Bittersmann, E.; Seely, G. R.; Gao, F.; Nieman, R. A.; Ma, X. C.; Demanche, L. J.; Hung, S.-C.; Luttrull, D. K.; Lee, S.-J.; Kerrigan, P. K. *J. Am. Chem. Soc.* **1993**, *115*, 11141−11152.
(11) Wasielewski, M. R.; Niemczyk, M. P.; Svec, W. A.; Pewitt, E. B. *J. Am. Chem. Soc.* **1985**, *107*, 5562−5563.
(12) Wasielewski, M. R.; Gaines, G. L., III; O'Neil, M. P.; Svec, W. A.; Niemczyk, M. P. *J. Am. Chem. Soc.* **1990**, *112*, 4559−4560.
(13) Wasielewski, M. R.; Gaines, G. L., III; O'Neil, M. P.; Niemczyk, M. P.; Svec, W. A. *Supramolecular arrays for the efficient conversion of light into chemical energy in the solid state*; Wasielewski, M. R., Gaines, G. L., III, O'Neil, M. P., Niemczyk, M. P., Svec, W. A., Eds.; Kluwer, 1992; pp 201−218.
(14) Wasielewski, M. R.; G. L. Gaines, I.; Wiederrecht, G. P.; Svec, W. A.; Niemczyk, M. P. *J. Am. Chem. Soc.* **1993**, *115*, 10442−10443.
(15) Li, L.; Shen, S.; Yu, Q.; Zhou, Q.; Xu, H. *J. Chem. Soc., Chem. Commun.* **1991**, 619.
(16) Batova, E. E.; Levin, P. P.; Shafirovich, V. Y. *New J. Chem.* **1990**, *14*, 269−271.

S0002-7863(96)00078-9 CCC: $12.00

makes it inherently difficult to study the stepwise nature of the charge separation. The formation of the various radical ion pair intermediates is usually inferred from a reduction of the fluorescence quantum yield and/or measurements of excited state lifetimes that are shortened relative to those of reference compounds in which electron transfer cannot occur, rather than by direct observations of the intermediate radical ion pairs using time-resolved optical absorption or electron paramagnetic resonance (TREPR) spectroscopy. Osuka and co-workers have circumvented this problem by using a pyromellitimide as either the primary or secondary acceptor.[17−23]

Triads that are based on donors and acceptors that are structurally and electronically simpler than porphyrins provide important insights into the charge separation process. For example, Verhoeven and co-workers have examined a number of interesting triad systems based on aniline electron donors and cyanoarene electron acceptors.[24−31] In addition, a number of triads that make use of the metal-to-ligand charge transfer (MLCT) excited states of ruthenium polypyridyl complexes, usually using viologen or diquat as the acceptor, have been studied.[32−36]

In keeping with the theme of using simple structures, aromatic diimides can be linked together using aryl diamines to yield linear, rod-like structures that have interest as potential molecular wires.[37] The principal degrees of conformational freedom in these molecules are restricted rotations about the single bonds that join the aryl spacers to the nitrogen atoms of the diimides. A distinguishing feature of the triads used for the studies presented here is their well-defined structure. The dimethylphenyl linkage between ANI and NI within **MeOAn-ANI-NI** and **An-ANI-NI** sterically hinders rotation about the single bonds joining these components in a rod-like structure. Rotation about the single C−N bond joining the piperazine rings of An and MeOAn to ANI is restricted by the peri hydrogen atom of the naphthalene ring. Moreover, the piperazine ring in compounds analogous to

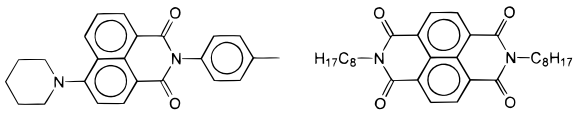

ANI **NI**

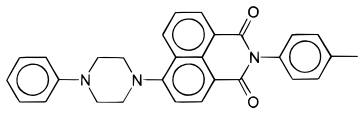

An-ANI

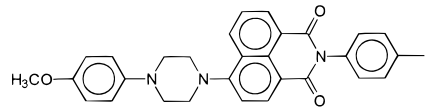

MeOAn-ANI

MeOAn-ANI-NI has been shown to strongly favor its chair conformation.[24,38] As a result, the distances and orientations between the electron donors and acceptors within the dyads and triads used in this study are restricted, thus providing a narrow distribution of values for the electronic coupling matrix element between the donors and acceptors.

Aromatic diimides typically undergo two reversible one-electron reductions to yield the corresponding radical anion and dianion.[39] The redox potentials for these processes vary as a function of the aromatic core of the diimides. Thus, employing different aromatic diimides can result in a significant negative ΔG for electron transfer between linked diimides. Moreover, the optical spectra of the stable radical anions of aromatic diimides, such as pyromellitimides and 1,4:5,8-tetracarboxynaphthalenediimides, possess sharp, distinct signatures that can be used to detect the presence of these ions using transient absorption spectroscopy.[40] This makes it possible to track electron movement in a multistep electron transfer process involving two or more diimides.

The lowest excited singlet state of the 4-aminonaphthalene-1,8-imide chromophore possesses significant charge transfer character. Measurements of the solvatochromism of its fluorescence emission spectrum suggest that its excited state dipole moment is 11 D.[41] Moreover, the direction of this excited state dipole in dyads **An-ANI**, **MeOAn-ANI,** and **ANI-NI** and in triads **An-ANI-NI** and **MeOAn-ANI-NI** is such that its positive end always lies near an electron donor and its negative end lies

(17) Osuka, A.; Nagata, T.; Maruyama, K.; Mataga, N.; Asahi, T.; Yamazaki, I.; Nishimura, Y. *Chem. Phys. Lett.* **1991**, *185*, 88−94.
(18) Osuka, A.; Nagata, T.; Kobayashi, F.; Zhang, R. P.; Maruyama, K.; Mataga, N.; Asahi, T.; Ohno, T.; Nozaki, K. *Chem. Phys. Lett.* **1992**, *199*, 302−308.
(19) Osuka, A.; Zhang, R.-P.; Maruyama, K.; Ohno, T.; Nozaki, K. *Chem. Lett.* **1993**, 1727−1730.
(20) Osuka, A.; Nakajima, S.; Maruyama, K.; Mataga, N.; Asahi, T.; Yamazaki, I.; Nishimura, Y.; Ohno, T.; Nozaki, K. *J. Am. Chem. Soc.* **1993**, *115*, 4577−4589.
(21) Osuka, A.; Yamada, H.; Maruyama, K.; Mataga, N.; Asahi, T.; Ohkouchi, M.; Okada, T.; Yamazaki, I.; Nishimura, Y. *J. Am. Chem. Soc.* **1993**, *115*, 9439−9452.
(22) Ohkohchi, M.; Takahashi, A.; Mataga, N.; Okada, T.; Osuka, A.; Yamada, H.; Maruyama, K. *J. Am. Chem. Soc.* **1993**, *115*, 12137−12143.
(23) Osuka, A.; Marumo, S.; Maruyama, K.; Mataga, N.; Ohkohchi, M.; Taniguchi, S.; Okada, T.; Yamazaki, I.; Nishimura, Y. *Chem. Phys. Lett.* **1994**, *225*, 140−145.
(24) Mes, G. F.; van Ramesdonk, H. J.; Verhoeven, J. W. *J. Am. Chem. Soc.* **1984**, *106*, 1335−1340.
(25) Brouwer, A. M.; Mout, R. D.; van den Brink, P. H. M.; van Ramesdonk, H. J.; Verhoeven, J. W.; Warman, J. M.; Jonker, S. A. *Chem. Phys. Lett.* **1991**, *180*, 556−562.
(26) Brouwer, A. M.; Mout, R. D.; van den Brink, P. H. M.; van Ramesdonk, H. J.; Verhoeven, J. W.; Jonker, S. A.; Warman, J. M. *Chem. Phys. Lett.* **1991**, *186*, 481−489.
(27) Brouwer, A. M.; Eijckelhoff, C.; Willemse, R. J.; Verhoeven, J. W.; Schuddeboom, W.; Warman, J. M. *J. Am. Chem. Soc.* **1993**, *115*, 2988−2989.
(28) van Dijk, S. I.; Wiering, P. G.; van Staveren, R.; van Ramesdonk, H. J.; Brouwer, A. M.; Verhoeven, J. W. *Chem. Phys. Lett.* **1993**, *214*, 502−506.
(29) Roest, M. R.; Lawson, J. M.; Paddon-Row, M. N.; Verhoeven, J. W. *Chem. Phys. Lett.* **1994**, *230*, 536−542.
(30) Willemse, R. J.; Verhoeven, J. W.; Brouwer, A. M. *J. Phys. Chem.* **1995**, *99*, 5753−5756.
(31) Dijk, S. I. v.; Wiering, P. G.; Groen, C. P.; Brouwer, A. M.; Verhoeven, J. W.; Schuddeboom, W.; Warman, J. M. *J. Chem. Soc., Faraday Trans.* **1995**, *91*, 2107−2114.
(32) Danielson, E.; Elliott, C. M.; Merkert, J. W.; Meyer, T. J. *J. Am. Chem. Soc.* **1987**, *109*, 2519−2520.
(33) Mecklenburg, S. L.; Peek, B. M.; Erickson, B. W.; Meyer, T. J. *J. Am. Chem. Soc.* **1991**, *113*, 8540−8542.
(34) Collin, J.-P.; Guillerez, S.; Sauvage, J.-P.; Barigelletti, F.; De Cola, L.; Flamigni, L.; Balzani, V. *Inorg. Chem.* **1991**, *30*, 4230−4238.
(35) Larson, S. L.; Cooley, L. F.; Elliott, C. M.; Kelley, D. F. *J. Am. Chem. Soc.* **1992**, *114*, 9504−9509.
(36) Harriman, A.; Odobel, F.; Sauvage, J.-P. *J. Am. Chem. Soc.* **1994**, *116*, 5481−5482.
(37) Dietz, T. M.; Stallman, B. J.; Kwan, W. S. V.; Penneau, J. F.; Miller, L. L. *J. Chem. Soc., Chem. Commun.* **1990**, 367−369.
(38) Dijkstra, G. D. H. *Rec. Trav. Chim. Pays-Bas* **1993**, *112*, 151−160.
(39) Kwan, W. S. V.; Penneau, J. F.; Miller, L. L. *J. Electroanal. Chem.* **1990**, *291*, 295−299.
(40) Viehbeck, A.; Goldberg, M. J.; Kovac, C. A. *J. Electrochem. Soc.* **1990**, *137*, 1460−1466.
(41) deSilva, A. P.; Gunaratne, H. Q. N.; Habib-Jiwan, J.-L.; McCoy, C. P.; Rice, T. E.; Soumillion, J.-P. *Angew. Chem., Int. Ed. Engl.* **1995**, *34*, 1728−1731.

near an electron acceptor. This orientation may facilitate subsequent electron transfer reactions by means of an electric field effect or by polarization of the surrounding solvent environment. Charge asymmetry within the lowest excited state of the bacteriochlorophyll dimeric donor in photosynthetic reaction centers has been implicated in the mechanism for charge separation in these proteins.[42−44]

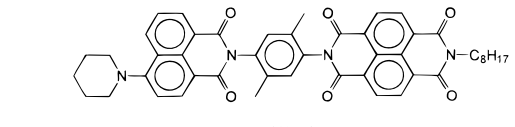

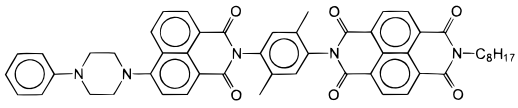

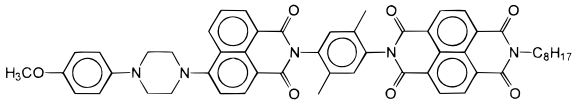

In this paper we present results on molecular triads that employ the combined strategies of using a rigid-rod aryl diimide electron acceptor and a photoreceptor possessing a charge transfer excited singlet state to achieve high quantum yield, long-lived charge separation in synthetically simple structures. These structures have the distinct advantage that the detailed mechanism of the charge separation can be readily discerned because all the relevant states, i.e., the excited singlet state and both ion pairs, are spectroscopically distinct from each other and are fully resolved by transient absorption spectroscopy. In a preliminary report we have shown that the long-lived radical ion pair and triplet state that results from charge recombination in **MeOAn-ANI-NI** exhibit spin polarization that closely mimics the spin dynamics observed in photosynthetic reaction centers.[45]

Results and Discussion

Steady-State Spectroscopy. The lowest energy optical transitions within the dyads and triads belong to the 4-aminonaphthalene-1,8-imide (ANI) chromophore. The spectroscopic properties of similar 4-aminonaphthalene-1,8-imide chromophores have been examined by other workers.[41,46−48] The presence of the amino substituent on the naphthalene ring radically changes the excited state characteristics of the molecule. In the absence of the amine the lowest energy electronic transition of the naphthalene-1,8-imide is a $\pi\pi^*$ transition. Adding the amine substituent to the 4-position of the naphthalene-1,8-imide results in a new lowest excited singlet state that is primarily charge transfer (CT) in nature.[41,47]

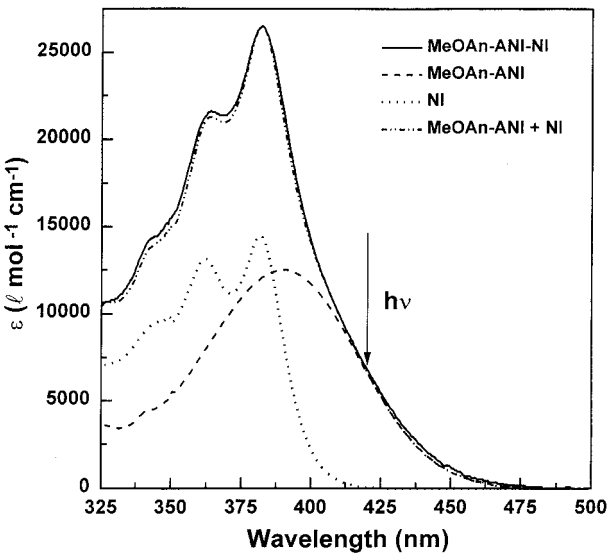

Figure 1. Ground state absorption spectra of **MeOAn-ANI-NI**, **MeOAn-ANI**, and **NI.** Also shown is the sum of the spectra of **MeOAn-ANI** and **NI**.

Table 1. Optical Absorption and Fluorescence Data

molecule	ANI absorption max. (nm)	fluorescence max. (nm)	quantum yield
ANI	399	498	0.91
An-ANI	385	515	0.48
MeOAn-ANI	390	572	0.035
ANI-NI	399[a]	501	0.18
An-ANI-NI	385[a]	513	0.12
MeOAn-ANI-NI	390[a]	502	0.006

[a] Based on the value of the corresponding molecule without NI.

Figure 1 shows the ground state absorption spectra in toluene of **MeOAn-ANI-NI**, **MeOAn-ANI**, and *N,N′*-di(*n*-octyl)naphthalene-1,8:4,5-diimide, **NI,** as well as the sum of the spectra of **MeOAn-ANI** and **NI**. Molecule **NI** serves as a reference molecule for the NI acceptor incorporated into the dyads and triads. Peak extinction coefficients (l mol^{-1} cm^{-1}) for ANI and NI in **MeOAn-ANI-NI** are 12 500 at 390 nm and 14 500 at 382 nm, respectively. Figure 1 shows that the spectrum of triad **MeOAn-ANI-NI** is very well matched by the simple sum of the spectra of its component chromophores. Attachment of the NI acceptor does not significantly perturb the CT absorption spectrum of ANI from that observed in dyad **MeOAn-ANI**. In an analogous way, the spectrum of triad **An-ANI-NI** (not shown) can be reconstructed from the spectra of **An-ANI** and **NI**, and the spectrum of dyad **ANI-NI** (not shown) can be reconstructed from the sum of the spectra of **ANI** and **NI**. In contrast, changing the nature of the substituents attached to the 4-nitrogen atom of the ANI chromophore changes the energy of its CT transition.[48] Thus, the CT transition in the molecules containing the MeOAn group is blue shifted 9 nm relative to that of **ANI**, while those containing the An group are blue-shifted 14 nm relative to that of **ANI**. Apart from the energies of their CT transitions, the spectra of the entire series have very similar shapes and extinction coefficients. These steady-state spectroscopic measurements in toluene are summarized in Table 1.

The ground state absorption spectra of the ANI and NI chromophores overlap somewhat in the molecules where both are present. In Table 1 the wavelength of the ANI absorption peak in molecules having both ANI and NI is given as that of the corresponding molecule not containing the NI component, e.g., the wavelength of the **MeOAn-ANI** peak is used for that

(42) Won, Y.; Friesner, R. A. *J. Phys. Chem.* **1988**, *92*, 2214−2219.
(43) Kirmaier, C.; Holten, D.; Bylina, E. J.; Youvan, D. C. *Proc. Natl. Acad. Sci. U.S.A.* **1988**, *85*, 7562−7566.
(44) McDowell, L. M.; Kirmaier, C.; Holten, D. *J. Phys. Chem.* **1991**, *95*, 3379−3383.
(45) Hasharoni, K.; Levanon, H.; Greenfield, S. R.; Gosztola, D. J.; Svec, W. A.; Wasielewski, M. R. *J. Am. Chem. Soc.* **1995**, *117*, 8055−8056.
(46) Viktorova, E. N.; Pereyaslova, D. G.; Yushko, E. G. *Russ. J. Phys. Chem.* **1966**, *40*, 962−965.
(47) Korol'kova, N. V.; Val'kova, G. A.; Shigorin, D. N.; Shigalevskii, V. A.; Vostrova, V. N. *Russ. J. Phys. Chem.* **1990**, *64*, 206−209.
(48) Alexiou, M. S.; Tychopoulos, V.; Ghorbanian, S.; Tyman, J. H. P.; Brown, R. G.; Brittain, P. I. *J. Chem. Soc., Perkin Trans. 2* **1990**, 837−842.

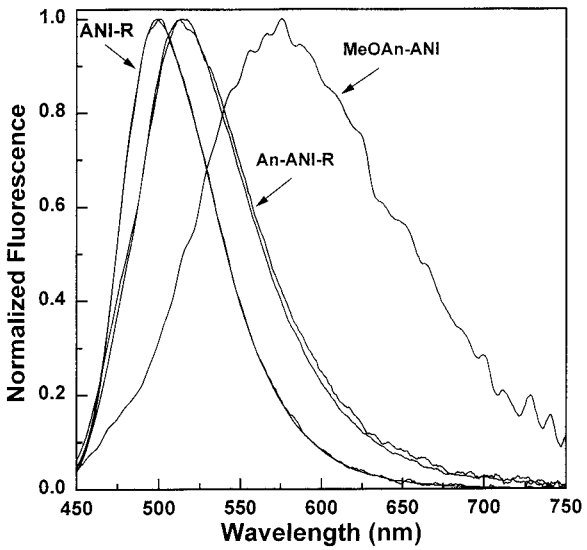

Figure 2. Normalized fluorescence spectra of **ANI**, **ANI-NI**, **An-ANI**, **MeOAn-ANI**, and **An-ANI-NI** in toluene. The fluorescence excitation wavelength is 445 nm.

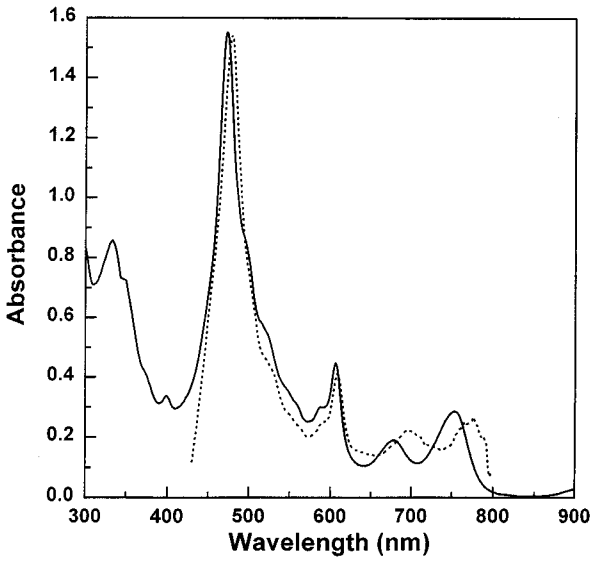

Figure 3. Solid line shows the steady-state absorption spectrum of electrochemically reduced **NI** in dimethylformamide. Also shown (dashed line) for comparison is the transient absorption spectrum of NI^- in **ANI-NI** in toluene 4 ns after excitation.

of **MeOAn-ANI-NI**. This is reasonable given the excellent reconstruction of the full triad spectra from the sums of the appropriate donor-ANI dyad and **NI** as described above. The ability to reconstruct the spectra of **ANI-NI** and the triads from the respective spectra of the compounds lacking NI and the spectrum of NI reference compound **NI** suggests that the electronic coupling between ANI and NI is weak, which is born out by the relatively slow electron transfer rates observed between those components in spite of the large driving force for the reaction (see below). Optical excitation at either 412 or 420 nm occurs on the red edge of the ANI chromophore and results in negligible excitation of the NI acceptor, 3.5% and 0.8%, respectively, with the MeOAn donor attached.

Fluorescence spectra were recorded and quantum yield measurements were made for all molecules, and the results are listed in Table 1. **ANI** is highly fluorescent in low polarity solvents and has a quantum yield of 0.91 in toluene. The fluorescence maximum of **ANI** in the higher polarity solvents tetrahydrofuran (THF) and butyronitrile (PrCN) red shifts by 15 and 29 nm, respectively, and is accompanied by a corresponding drop in fluorescence quantum yield to 0.72 and 0.25, respectively. This classic behavior is characteristic for charge transfer excited states. Figure 2 shows the normalized emission spectra ($\lambda_{exc} = 445$ nm) of **ANI**, dyads **An-ANI**, **MeOAn-ANI**, and **ANI-NI**, and triad **An-ANI-NI** in toluene. The fluorescence from triad **MeOAn-ANI-NI** is very weak and is not shown. The normalized fluorescence spectra of **ANI** and **ANI-NI** are identical, which indicates that both the identity and nature of the fluorescing state, i.e. ^{1*}**ANI**, are unperturbed by the addition of the NI acceptor. Similarly, the spectra of **An-ANI** and **An-ANI-NI** are identical, but their emission maxima are red shifted by 16 nm from that of the **ANI** CT state. As will be discussed in detail below, the large fluorescence quantum yield of **An-ANI** ($\phi = 0.48$) is inconsistent with the transient absorption data unless this fluorescence is charge recombination fluorescence, presumably from $\mathbf{An}^+$-$\mathbf{ANI}^-$. The peak of the fluorescence spectrum of **MeOAn-ANI** is red shifted 74 nm from that of **ANI** and is much broader. The shift and width of this spectrum, combined with a fluorescence quantum yield that is once again significantly higher than that expected on the basis of transient absorption measurements (see below), show that the emission from **MeOAn-ANI** is due to charge recombination fluorescence from $\mathbf{MeOAn}^+$-$\mathbf{ANI}^-$ rather than CT fluorescence from ^{1*}ANI itself.

Figure 3 shows the spectrum of electrochemically reduced **NI** in dimethylformamide. Also shown is the transient absorption spectrum of NI^- within $\mathbf{ANI}^+$-$\mathbf{NI}^-$ in toluene at 4 ns after excitation (see below). Despite the fact that the data were obtained in different solvents, the resemblance of the transient spectrum to the steady-state one is striking.

Energetics of Charge Separation within the Dyads and Triads. Accurate determinations of the energy levels of ion pair states in donor−acceptor molecules in low polarity media are difficult. Frequently, the CT or ion pair states produced by photochemical charge separation recombine nonradiatively to their ground states. Thus, direct spectroscopic information about the energy levels of the charge separated states is not available. In polar media the sum of the thermodynamic potentials for oxidation of the donor and reduction of the acceptor often give a reasonable estimate of the ion pair state energy. However, for low polarity media one must resort to modeling the change in solvation energy of the ions that occurs when the ions are taken from the high static dielectric constant medium in which the redox potentials are measured to one of low dielectric constant. Weller developed an expression based on the Born dielectric continuum model of the solvent to determine the ΔG of formation for an ion pair in a solvent of arbitrary polarity[49]

$$\Delta G = E_{ox} - E_{red} - \frac{e^2}{r_{12}\epsilon_s} + e^2\left(\frac{1}{2r_1} + \frac{1}{2r_2}\right)\left(\frac{1}{\epsilon_s} - \frac{1}{\epsilon_{sp}}\right) \quad (1)$$

where E_{ox} and E_{red} are, respectively, the oxidation and reduction potentials of the donor and acceptor in a high polarity solvent with a static dielectric constant ϵ_{sp}, e is the charge of the electron, r_{12} is the ion pair distance, r_1 and r_2 are the ionic radii, and ϵ_s is the static dielectric constant of a solvent with arbitrary polarity. The term involving the ion pair distance is simply the coulombic interaction of the ions. The last term accounts for the lesser ability of the lower polarity solvents to stabilize charges as compared to the high polarity solvent used in the electrochemical measurements. It is well known that eq 1

(49) Weller, A. *Z. Phys. Chem.* **1982**, *133*, 93−98.

overestimates the degree of destabilization of an ion pair in low polarity solvents relative to those with high polarity.[50]

To more accurately determine the ion pair state energies for the dyads and triads described in this work we will use a more direct spectroscopic/electrochemical method that makes use of the fact that **ANI**, **An-ANI**, and **MeOAN-ANI** possess ion pair states that undergo radiative recombination. Redox potentials for the various donors and acceptors were determined in PrCN with 0.1 M tetra-*n*-butylammonium perchlorate and are given in Table 2. The free energy of formation of the charge separated state and the total reorganization energy for its formation can be determined from eqs 2 and 3, if the energies of the charge transfer absorption and emission transitions, E_a and E_e, can be identified, and if one assumes that the potential surfaces describing the ground and charge separated states of the molecule are similar.[51]

$$\Delta G = \frac{E_a + E_e}{2} \tag{2}$$

$$\lambda = \frac{E_a - E_e}{2} \tag{3}$$

Using the absorption and emission data for **ANI** found in Table 1, eqs 2 and 3 yield $\Delta G = 2.80$ eV and $\lambda = 0.31$ eV, respectively. The total reorganization energy is $\lambda = \lambda_i + \lambda_s$, where λ_i is the reorganization energy due to the internal modes of the molecule, and λ_s is due to the reorganization of the solvent. Marcus has shown that

$$\lambda_s = e^2\left(\frac{1}{2r_1} + \frac{1}{2r_2} - \frac{1}{r_{12}}\right)\left(\frac{1}{\epsilon_o} - \frac{1}{\epsilon_s}\right) \tag{4}$$

where e, r_{12}, r_1, r_2, and ϵ_s are defined above, and ϵ_o is the high frequency dielectric constant of the solvent. For toluene, $\epsilon_o \cong \epsilon_s$, so that eq 4 yields $\lambda_s \cong 0$. Thus, $\lambda_i = 0.3$ for **ANI**. Since this value is typical of organic π donors and acceptors,[52] we assume that a similar value of λ_i is valid for electron transfer reactions involving molecules of similar structural type, such as **An-ANI** and **MeOAn-ANI**. The long wavelength emission in these molecules is due to radiative recombination of the corresponding ion pairs, **An**$^+$**-ANI**$^-$ and **MeOAn**$^+$**-ANI**$^-$. Unfortunately, it is difficult to clearly discern a corresponding charge transfer absorption because of the presence of the intense CT absorption of the ANI chromophore. Nevertheless, eqs 2 and 3 can be combined to yield

$$\Delta G = E_e + \lambda \tag{5}$$

Since the data for **ANI** show that $\lambda = 0.3$, using this value and the respective emission energies of **An-ANI** and **MeOAn-ANI**, Table 1, eq 5 yields $\Delta G = 2.72$ and 2.48 eV, respectively. The 0.24 eV difference in the energy levels of **An**$^+$**-ANI**$^-$ and **MeOAn**$^+$**-ANI**$^-$ determined spectroscopically agrees well with the 0.26 V difference in oxidation potential between the An and MeOAn electron donors, Table 2.

The free energies of the charge shift reactions within the triads can be determined by taking into account the change in redox potential for reduction of NI versus ANI and the change in Coulomb energy needed to separate the charges the additional distance. *The energy changes required to solvate the charges of the ion pair are already included in the spectroscopically determined energies of the initial ion pair state.* Thus, the energies of the fully charge separated states in the triads are given by

$$\Delta G_{IP2} = \Delta G_{IP1} + E_{red}(\text{ANI}) - E_{red}(\text{NI}) + \frac{e^2}{\epsilon_s}\left(\frac{1}{r_{IP1}} - \frac{1}{r_{IP2}}\right) \tag{6}$$

where ΔG_{IP1} and ΔG_{IP2} are the free energies of formation of the initial ion pair state (i.e., donor$^+$-ANI$^-$-NI) and the final ion pair state (i.e., donor$^+$-ANI-NI$^-$), respectively, E_{red}*(ANI)* and E_{red}*(NI)* are the potentials for reduction of ANI and NI, respectively, and r_{IP1} and r_{IP2} are the corresponding distances between the ions in ion pairs 1 and 2, respectively. Equation 6 assumes that E_{red}*(ANI)* $- E_{red}$*(NI)* is the same in toluene and PrCN. The fact, noted above, that the energy difference between **An**$^+$**-ANI**$^-$ and **MeOAn**$^+$**-ANI**$^-$ determined spectroscopically in toluene is almost the same as the redox potential difference for oxidation of MeOAn and An in PrCN suggests that this assumption is reasonable. The values of r_{IP1} and r_{IP2} were determined from energy minimized structures of the dyads and triads using force-field calculations.[53] The solvent dielectric constants are from ref 54. The energies of **An**$^+$**-ANI-NI**$^-$ and **MeOAn**$^+$**-ANI-NI**$^-$ in toluene using eq 6 are given in Table 3 along with the values calculated using the method of Weller. For the Weller calculation ionic radii of 3.5 Å were used. The data in Table 3 show that the Weller method consistently overestimates the energies of the ion pair states by about 0.5 eV in toluene.

The accuracy of the spectroscopic/electrochemical method for determining the ion pair state energy for **MeOAn**$^+$**-ANI-NI**$^-$ can be checked by an independent measurement. We have previously observed the ion pair state **MeOAn**$^+$**-ANI-NI**$^-$ in toluene at 150 K by TREPR.[55] In the same experiment we observed that the lowest excited triplet state of **MeOAn-ANI-NI** is in equilibrium with **MeOAn**$^+$**-ANI-NI**$^-$, which at 150 K suggests that these states are nearly degenerate. Phosphorescence measurements show that the lowest excited triplet state of **MeOAn-ANI-NI** is localized on NI with an energy of 2.03

Table 2. Redox Potentials of Triad Components Measured in Butyronitrile (V vs SCE)

part	oxidation	reduction
MeOAn (donor)	0.79	
An (donor)	1.05	
ANI (chromophore)	1.20	−1.41
NI (acceptor)		−0.53

Table 3. Energy Levels with Respect to the Ground State

state	r_{12} (Å)	*E* (eV) spectroscopic method	*E* (eV) Weller method
^{1}*ANI	3.3	2.80	
An$^+$**-ANI**$^-$	7.7	2.72	3.24
MeOAn$^+$**-ANI**$^-$	7.7	2.48	2.98
ANI$^+$**-NI**$^-$	15.2	2.42	2.89
An$^+$**-ANI-NI**$^-$	19.1	2.31	2.83
MeOAn$^+$**-ANI-NI**$^-$	19.1	2.07	2.57

(50) Warman, J. M.; Smit, K. J.; Jonker, S. A.; Verhoeven, J. W.; Oevering, H.; Kroon, J.; Paddon-Row, M. N.; Oliver, A. M. *Chem. Phys.* **1993**, *170*, 359−380.

(51) Gould, I. R.; Noukakis, D.; Gomez-Jahn, L.; Young, R. H.; Goodman, J. L.; Farid, S. *Chem. Phys.* **1993**, *176*, 439−456.

(52) Closs, G. L.; Miller, J. R. *Science* **1988**, *240*, 440−447.

(53) Ion pair distances were estimated from structures calculated using a modified MM2 force field and AM1 MO calculations were performed within Hyperchem (Hypercube, Waterloo, Ontario) .

(54) Riddick, J. A.; Bunger, W. B.; Sakano, T. K. *Organic Solvents: Physical Properties and Methods of Purification*, 4th ed.; John Wiley & Sons: New York, 1986.

(55) Hasharoni, K.; Levanon, H.; Greenfield, S. R.; Gosztola, D. J.; Svec, W. A.; Wasielewski, M. R. *Isr. J. Chem.* **1996**, *submitted.*

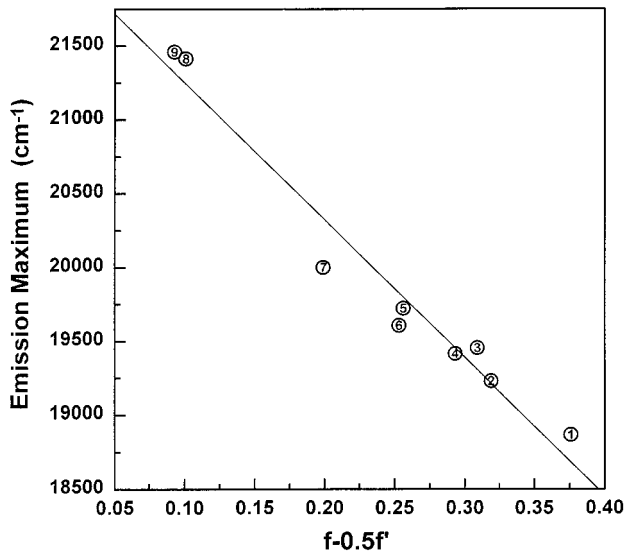

Figure 4. Plot of the fluorescence emission maximum of **ANI** as a function of the solvent polarity factor as given in eq 7, where $f = (\epsilon-1)/(2\epsilon+1)$ and $f' = (n^2-1)/(2n^2+1)$. The following solvents were used: (1) butyronitrile, (2) dichloromethane, (3) tetrahydrofuran, (4) ethyl acetate, (5) diethyl ether, (6) chloroform, (7) trichloroethylene, (8) methylcyclohexane, and (9) hexane.

eV. Thus, the two experiments imply that the energy of **MeOAn$^+$-ANI-NI$^-$** is also about 2.03 eV at 150 K. This agrees very well with the 2.07 eV energy of **MeOAn$^+$-ANI-NI$^-$** determined in toluene at room temperature using eq 6. The weak temperature dependence of the **MeOAn$^+$-ANI-NI$^-$** state energy is an expected consequence of the fact that $\lambda_s \cong 0$ at both 150 K and room temperature.

The properties of the emissive CT states of **ANI**, **AnANI**, and **MeOAnANI** provide essential information that can be used to further analyze the energetics of charge separation and recombination in these molecules. The value of the excited state dipole moment for **ANI** was determined from the slope of a plot (Figure 4) of the solvatochromic shift of the CT emission maximum, $\bar{\nu}$ of ANI as a function of the solvent polarity parameter as described by eq 7[56−58]

$$\bar{\nu} = -\frac{2\mu_e^2}{hca^3}\left[\frac{\epsilon_s - 1}{2\epsilon_s + 1} - \frac{n^2 - 1}{4n^2 + 2}\right] \quad (7)$$

where h is Planck's constant, c is the speed of light, n is the refractive index of the medium, ϵ_s is static dielectric constant of the solvent, μ_e is the dipole moment of the CT state, and a is the semimajor axis of an ellipsoidal cavity containing **ANI**. For $a = 5$ Å, $\mu_e = 11.1 \pm 0.4$ D. This value is in good agreement with an earlier assessment of 11D for the excited state dipole moment in *N*-alkylated derivatives of 4-amino-naphthalene-1,8-imide.[41] The **ANI** CT state produces an 11.1 D dipole moment if a unit charge is transferred over a distance of 2.3 Å within **^{1*}ANI**. However, if the degree of charge separation within the excited state is less than unity, this distance will be greater.

Equation 6 can be rewritten as eq 8 and used to test whether the degree of charge separation within **^{1*}ANI** is indeed unity

$$\Delta G_{IP2} = \Delta G_{IP1} - (E_{OX1} - E_{OX2}) + \frac{e^2}{\epsilon_s}\left(\frac{q^2}{r_{IP1}} - \frac{1}{r_{IP2}}\right) \quad (8)$$

where ΔG_{IP1} is the energy of **^{1*}ANI**, ΔG_{IP2} is the predicted energy of the **An$^+$-ANI$^-$** or **MeOAn$^+$-ANI$^-$** ion pairs, E_{OX1} is the oxidation potential of **ANI**, E_{OX2} is the oxidation potential of the respective An or MeOAn donors, r_{IP1} is the 2.3 Å charge separation distance within **^{1*}ANI** that is necessary to account for its excited state dipole moment assuming unity charge transfer (see above), r_{IP2} is the 7.7 Å ion pair distance within **An$^+$-ANI$^-$** or **MeOAn$^+$-ANI$^-$**, and q is the fractional degree of charge separation within **^{1*}ANI**. Using these data and assuming unity charge separation ($q = 1$), eq 8 predicts that the energies for **An$^+$-ANI$^-$** and **MeOAn$^+$-ANI$^-$** are 4.48 and 4.21 eV, respectively. These values are about 1.8 eV higher than the actual values determined spectroscopically, Table 3. This suggests that the assumed 2.3 Å charge separation distance within **^{1*}ANI** is too small, which, in turn, suggests that the degree of charge separation within **^{1*}ANI** is less than unity.

The effective distance across which the charge separation occurs within **^{1*}ANI**, r_{IP1}, is related to q and the measured dipole moment of **^{1*}ANI**, μ_e, by $r_{IP1} = \mu_e/4.8q$, if the units of r_{IP1} and μ_e are angstroms and debyes, respectively. Substituting this expression for r_{IP1} into eq 8 and solving for q yields eq 9

$$q = \left[\frac{\mu_e}{4.8}\cdot\left(\frac{\epsilon_s(\Delta G_{IP2} - \Delta G_{IP1} + E_{OX1} - E_{OX2})}{e_o^2} + \frac{1}{r_{IP2}}\right)\right]^{1/3} \quad (9)$$

Using the redox potentials for ANI and the An and MeOAn donors listed in Table 2, and the state energies of **An$^+$-ANI$^-$** and **MeOAn$^+$-ANI$^-$** given in Table 3, eq 9 gives $q = 0.7$ using either set of data. Thus, charge separation within **^{1*}ANI** is about 70% complete, which yields an effective charge separation distance within **^{1*}ANI** of 3.3 Å. This distance agrees well with the charge separation distances within **ANI** estimated by AM1 MO calculations of its cation and anion radicals.[53]

In a similar manner, using $q = 0.7$ for the degree of charge separation within **^{1*}ANI**, eq 9 can be used to determine the ion pair state energy for **ANI$^+$-NI$^-$**. Using eq 9 with an ion pair distance of 15.2 Å for **ANI$^+$-NI$^-$** yields $\Delta G = 2.42$ eV.

Ultrafast Charge Separation and Recombination Reactions. The various pathways available for the lowest excited singlet state of triad **MeOAn-ANI-NI** after photoexcitation are shown in Scheme 1. The numbers are the time constants for the various processes directly measured for triad **MeOAn-ANI-NI**, while those in parentheses were measured for the most appropriate reference compound (see below).

The transient spectra of **ANI**, dyads **MeOAn-ANI** and **ANI-NI**, and triad **MeOAn-ANI-NI** at 4 ps, 40 ps, and 4 ns after the 420 nm excitation pulse are shown in Figure 5. The spectrum of **ANI** is dominated by a strong transient absorption at 450 nm due to excited state absorption of ^{1*}ANI and a stimulated emission band peaked at 510 nm. The apparent ~10 nm red shift of the peak of the stimulated emission with respect to that of the steady-state fluorescence is an artifact of the transient absorption spectrum being a superposition of excited state−excited state absorption and stimulated emission; i.e., the existence of excited state−excited state absorption at 500 nm causes the observed maximum of the stimulated emission band to shift to the red of its true value. There is also a broad, weak excited state−excited state absorption to the red of 650 nm. At 483 nm, the transient spectrum crosses zero, with the excited state absorption exactly canceling the stimulated emission. This zero-crossing point does not change as a function of time, and

(56) Lippert, E. *Z. Naturforsch.* **1955**, *10a*, 541−546.
(57) Mataga, N.; Kaifu, Y.; Koizumi, M. *Bull. Chem. Soc. Jpn.* **1956**, *29*, 465−470.
(58) Beens, H.; Knibbe, H.; Weller, A. *J. Chem. Phys.* **1967**, *47*, 1183−1184.

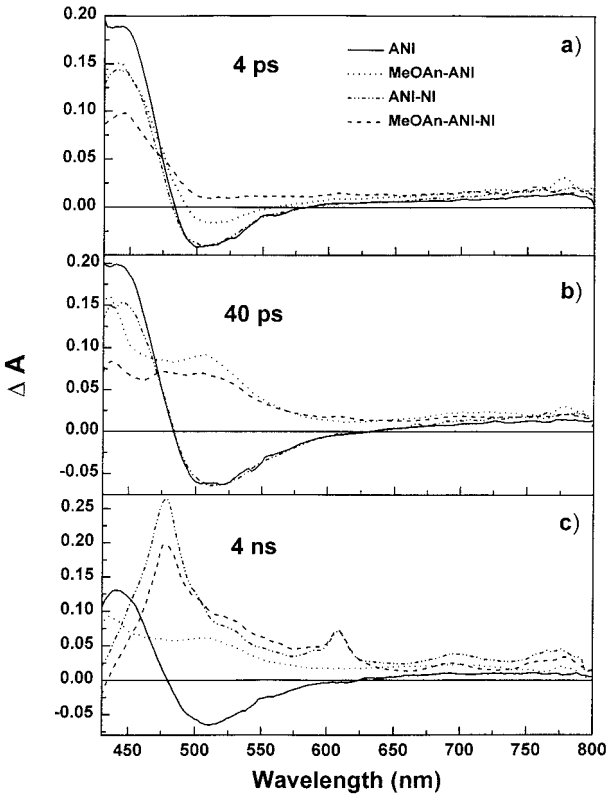

Figure 5. Transient absorption spectra of **MeOAn-ANI-NI**, **MeOAn-ANI**, **ANI-NI**, and **ANI** pumped at 420 nm. (a) 4 ps after excitation: all four molecules show ^{1*}ANI characteristics; (b) 40 ps after excitation: the two molecules containing the MeOAn component show the characteristic 510-nm $MeOAn^+$ absorption. (c) 4 ns: the strong 480-nm NI^- band has appeared in the two molecules containing the NI component.

Scheme 1

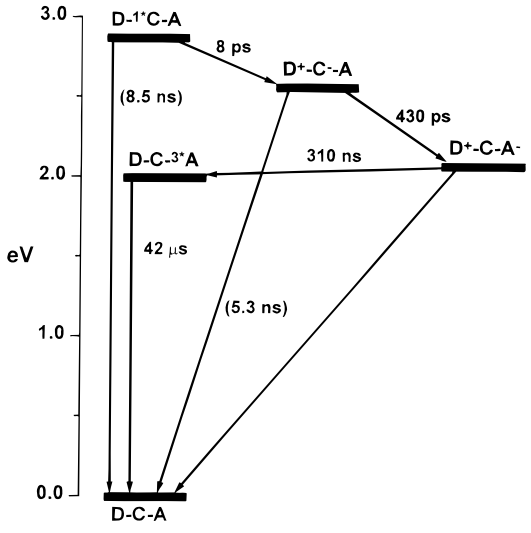

a kinetic scan of **ANI** run at 483 nm is essentially flat. Thus with the dyads and triads, probing at ~483 nm will allow the electron transfer kinetics to be seen without any contribution from ^{1*}ANI. This wavelength is especially convenient as it is near the absorption maximum for both the donor$^+$ and NI^- states.

The transient absorption kinetics of **^{1*}ANI** at 450 nm (λ_{pump} = 412 nm) can be seen in Figure 6. The measured rise is not quite instrument-response limited, being somewhat masked by the intrinsic response of toluene. The excited state decays with an 8.5 ns lifetime. The same decay time was observed by time-resolving the fluorescence decay with a multichannel plate photomultiplier tube (1.0-ns FWHM instrument response).

Table 4. Time Constants for Formation and Decay of Excited and Ionic States in Toluene

initial state	final state	formation time constant (ns)	decay time constant (ns)
ANI	**^{1*}ANI**		8.5
An-^{1*}ANI	**An^+-ANI^-**	0.019	5.0
MeOAn-^{1*}ANI	**$MeOAn^+$-ANI^-**	0.011	5.3
^{1*}ANI-NI	**ANI^+-NI^-**	1.4	150
An-^{1*}ANI-NI	**An^+-ANI^--NI**	0.016	
An^+-ANI^--NI	**An^+-ANI-NI^-**	1.6	150
MeOAn-^{1*}ANI-NI	**$MeOAn^+$-ANI^--NI**	0.008	
$MeOAn^+$-ANI^--NI	**$MeOAn^+$-ANI-NI^-**	0.43	310

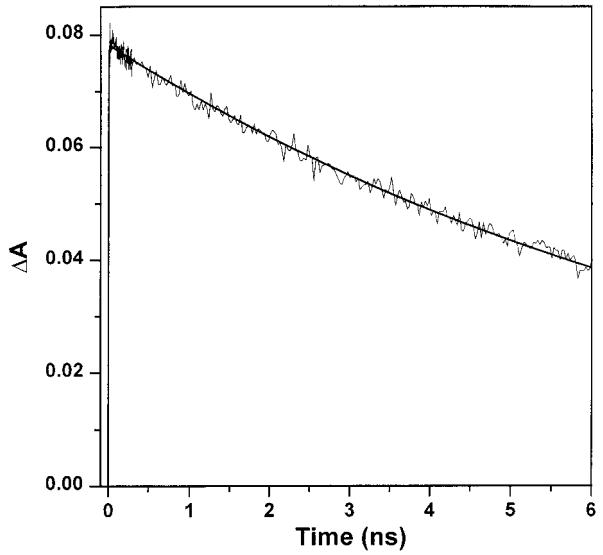

Figure 6. Transient absorption kinetics of **ANI** in toluene probed at 450 nm. The 8.5-ns decay is that of **^{1*}ANI**. The fit to the data is also shown.

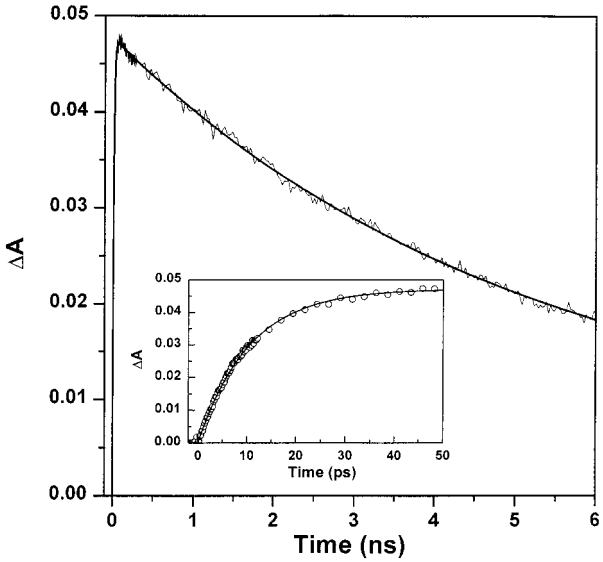

Figure 7. Transient absorption kinetics of **MeOAn-ANI** in toluene probed at 500 nm. The 5.3-ns decay is charge recombination, and the inset shows the 11-ps formation time of the ion pair state. The fit to the data is also shown.

The transient absorption kinetics for dyad **MeOAn-ANI** at 500 nm (λ_{pump} = 412 nm) can be seen in Figure 7. There is an 11-ps rise (see inset), followed by a 5.3-ns decay. The risetime reflects the time for electron transfer from the MeOAn donor

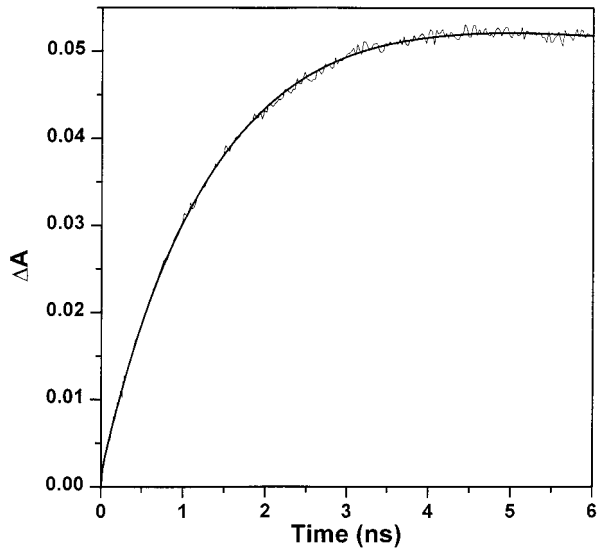

Figure 8. Transient absorption kinetics of **ANI-NI** in toluene probed at 483 nm. The 1.4-ns rise is the formation of the ion pair state. The fit to the data is also shown.

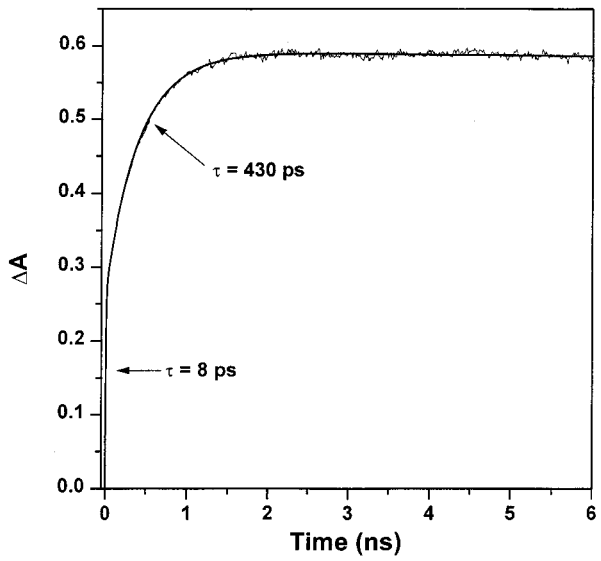

Figure 9. Transient absorption kinetics of **MeOAn-ANI-NI** in toluene probed at 483 nm. The biexponential rise shows the formation of the primary and final ion pair states. The fit to the data is also shown.

to the ANI chromophore, which here acts as the acceptor. The 5.3-ns decay is the time for back electron transfer to the ground state. Although the time for charge recombination is not far from the time for the decay of ^{1*}ANI in **ANI**, the transient spectra are unambiguous as to the existence of a different electronic state. At 4 ps, before significant electron transfer has occurred, the transient spectrum of **MeOAn-ANI** looks very similar to that of **ANI** (i.e., both are ^{1*}ANI). By 40 ps, however, the spectrum is radically different from that of ^{1*}ANI. There is now a sharp peak at 440 nm and a broad band to the red at 510 nm. The 510 nm band is due to absorption of the $MeOAn^+$ cation radical.[59,60] The sharp peak at 440 nm is due to the ANI^- anion (the exact nature of the blue edge of this peak is obscured by scatter from the blue pump beam, which appears as a negative ΔA). The presence of the anion absorption peak at roughly the same location as the ^{1*}ANI excited state absorption is not surprising, as the two transitions involve similar electronic states. The simple single-exponential decay of the charge separated state is consistent with a comparison of the 40 ps and 4 ns spectra. The features are identical, with the only difference being the population decay. From the kinetic data, the quantum yield for charge transfer is calculated to be unity. The fluorescence quantum yield of **MeOAn-ANI** ($\phi = 0.035$) implies a forward electron transfer time of 340 ps, which is over an order of magnitude slower than the rate observed by the transient absorption experiment. As discussed above, this discrepancy, combined with the spectral features of the fluorescence, indicate that it is charge recombination fluorescence from **MeOAn$^+$-ANI$^-$** and therefore cannot be used to calculate the rate constant for charge separation.

The kinetics of dyad **ANI-NI** at 483 nm can be seen in Figure 8. A slow, 1.4-ns rise is observed, corresponding to electron transfer from the excited chromophore to the acceptor, forming ANI^+ and NI^-. There is no back electron transfer observed on the time scale of the experiment. The transient spectra show the transition from ^{1*}ANI to NI^-. At 4 and 40 ps, the spectra are virtually identical to those of **ANI**. At 4 ns, the spectrum clearly shows the presence of the NI^- anion, as can be seen by comparing the transient spectrum with the spectrum of electrochemically reduced NI (see Figure 3). Even the blue shoulder of the 600-nm peak and the two small, broad peaks to the red 650 nm are discernible in the transient spectra. There is no apparent significant contribution from ANI^+, at least in this spectral region. The quantum yield for charge separation is 0.86 as calculated from the kinetic data. The fluorescence quantum yield of **ANI-NI** is 0.18. This predicts a forward electron transfer time of 2.2 ns, which is consistent with the transient absorption data.

The well-defined behavior of the three reference compounds allows us to unambiguously determine the electron transfer behavior of the triad molecule **MeOAn-ANI-NI**. The kinetics at 483 nm can be seen in Figure 9. There is a fast rise of 8 ps corresponding to electron transfer from the donor to the chromophore, resulting in **MeOAn$^+$-ANI$^-$-NI**. This is followed by a dark electron transfer from the chromophore anion to the acceptor, giving the giant dipole state **MeOAn$^+$-ANI-NI$^-$**. This subsequent charge shift reaction occurs with a rise time of 430 ps. The nature of the two electron transfer steps is clear when the transient spectra are compared to those of the reference compounds. At 4 ps, relatively little electron transfer has occurred, and the spectrum looks like ^{1*}ANI. At 40 ps, the primary charge separation is complete, and the spectrum looks like that of **MeOAn$^+$-ANI$^-$** within dyad **MeOAn-ANI**. Finally, at 4 ns the spectrum is dominated by NI^-, but the peak is broadened on the red side (as compared to the **ANI$^+$-NI$^-$** spectrum within dyad **ANI-NI**) by the presence of the $MeOAn^+$ cation in the triad. The quantum yield for the two-step charge separation process is 0.92 and is given by $\phi_{total} = \phi_1\phi_2$, where ϕ_1 is the quantum yield for primary charge separation (unity) and $\phi_2 = 0.92$ is the quantum yield for the secondary charge shift. The value of ϕ_2 is calculated assuming that the rate of charge recombination of the primary ion pair state is the same as that measured in the appropriate reference compound; i.e., $k_{CR} = (5.3\text{ ns})^{-1}$ from dyad **MeOAn-ANI**. The fluorescence quantum yield for **MeOAn-ANI-NI** is 0.006, which predicts a forward electron transfer time of 55 ps. The fluorescence is actually a combination of excited CT state fluorescence from ^{1*}ANI before the primary charge transfer step and charge recombination fluorescence from the initial ion pair state **MeOAn$^+$-ANI$^-$-NI**. From kinetic data of this triad and the kinetic and fluorescence data of the reference compounds, a

(59) Kimura, K.; Yoshinaga, K.; Tsubomura, H. *J. Phys. Chem.* **1967**, *71*, 4485−4491.

(60) Hester, R. E.; J. Williams, K. P. *J. Chem. Soc., Perkin Trans. II* **1982**, 559−563.

fluorescence quantum yield of ~0.004 is predicted, in good agreement with the measured value.

Aniline was used as a donor instead of MeOAn in dyad **An-ANI** and triad **An-ANI-NI**. Although An is a 0.26 eV weaker donor than MeOAn, forward electron transfer as measured by the transient absorption kinetics at 483 nm still has a fast rise time of only 19 ps. The transient absorption spectrum at 75 ps is clearly different from that at 3 ps (data not shown), which looks identical to that of **ANI** and is due to ^{1*}ANI. At 75 ps, there is still a stimulated emission band (peaked at ~560 nm), though it is ~50 nm redder than that of ^{1*}ANI. A virtually identical spectrum (other than population decay) is observed at 4 ns. As discussed above, the stimulated emission and steady-state fluorescence of dyad **An-ANI** is due to charge recombination fluorescence of the charge separated species An^+-ANI^-. The bathochromic shift of the stimulated emission peak with respect to the steady-state fluorescence maximum results, as described above for **ANI**, from the superposition of stimulated emission and excited state-excited state absorption features. The larger magnitude of the shift for **An-ANI** as compared to **ANI** is due to the presence of the An^+ peak at ~500 nm in the dyad spectrum. Because the charge separated state is formed with unity quantum yield, the quantum yield for charge recombination fluorescence is simply the measured fluorescence quantum yield; i.e., $\phi = 0.48$. The decay time of the ion pair state is 5 ns.

The data for triad **An-ANI-NI** is completely consistent with the description of the behavior of dyad **An-ANI** given above. Transient absorption kinetics (data not shown) at 483 nm show a fast 16-ps rise followed by a much slower 1.6-ns rise. The transient absorption spectrum at 75 ps is virtually identical to that of $\mathbf{An}^+$-$\mathbf{ANI}^-$ within dyad **An-ANI**, indicating that $\mathbf{An}^+$-$\mathbf{ANI}^-$-**NI** is formed with a 16-ps time constant, slightly faster than in the dyad. The spectrum at 6 ns is dominated by NI^-, with some broadening on the red edge of the 478-nm peak due to the presence to the An^+ cation. As with triad **MeOAn-ANI-NI**, the quantum yield for the initial charge separation step in **An-ANI-NI** is unity. The quantum yield for the secondary charge shift reaction (and hence the total quantum yield for formation of the giant dipole state) is 0.76. As discussed above, the fluorescence spectrum of triad **An-ANI-NI** is identical to that of dyad **An-ANI**, indicating that the fluorescence of the triad is also due to charge recombination from the $\mathbf{An}^+$-$\mathbf{ANI}^-$ ion pair state, which occurs in competition with the secondary charge shift reaction. The fluorescence quantum yield of triad **An-ANI-NI** is 0.18 and is fully consistent with the description given above. Given the 5-ns lifetime of the charge separated state and a quantum yield for charge recombination fluorescence of 0.48 for dyad **An-ANI**, one calculates a 1.6-ns time constant for the secondary charge shift reaction in the triad, exactly matching the value from the transient absorption experiments.

Slow Charge Recombination Reactions. The long time kinetics of triad **MeOAn-ANI-NI** at 480 nm can be seen in Figure 10. Degassed samples show a biexponential decay, with a fast component of ~310 ns and a slow component (see inset) of ~42 μs. Nondegassed samples do not have the slow component and decay to the baseline within 2 μs. The disappearance of the slow component in the nondegassed samples allows assignment of that component to a triplet state formed from recombination of the final ion pair state. This triplet state, which is localized on NI,[45] is rapidly quenched in the presence of O_2. The 310-ns component is therefore the lifetime of the giant dipole state and is basically unaffected by O_2.

Triad **MeOAn-ANI-NI** has been examined in toluene by transient dc conductivity techniques.[61] The final ion pair state

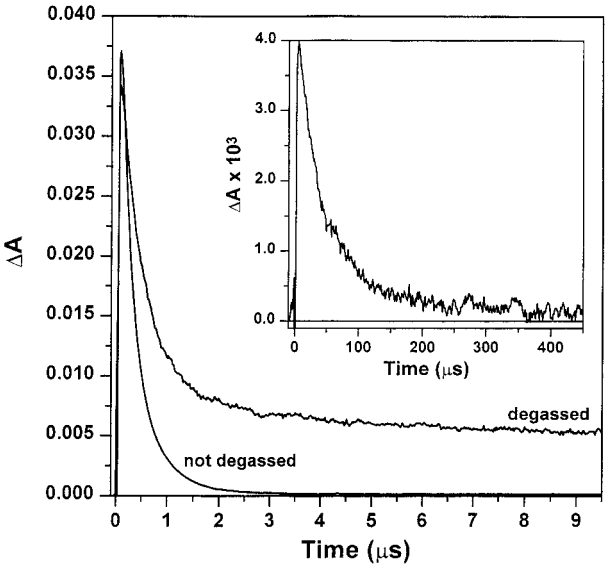

Figure 10. Microsecond transient absorption kinetics of **MeOAn-ANI-NI** in toluene probed at 480 nm (λ_{pump} = 416 nm). Both gassed and degassed samples are shown. The main decay is charge recombination of the final charge transfer species. Inset shows the triplet decay to the ground state for the degassed sample (note different time scale).

was measured to have a dipole moment of 87 ± 6 D. This corresponds to an ion pair distance of 18.1 Å, which is very close to the 19.1 Å distance determined from the energy minimized structure of **MeOAn-ANI-NI.**[53] Although the time resolution of the transient conductivity experiment did not allow determination of the forward electron transfer kinetics, the lifetime of the giant dipole state was measured to be 290 ns, in good agreement with the transient absorption data.

Electronic Coupling. The fact that $\mathbf{An}^+$-$\mathbf{ANI}^-$ and $\mathbf{MeOAn}^+$-$\mathbf{ANI}^-$ each possess a radiative recombination pathway back to their respective ground states makes it possible to use the characteristics of this emission process to determine the electronic coupling matrix element for this reaction. It has been shown previously that the radiative rate constant for CT emission can be related to the electronic matrix element V coupling the ground and CT state, and the change in static dipole moment between these two states, $\Delta\mu$, using eq 10[56-58]

$$k_r = \frac{64\pi^4}{3h^2c^3} \cdot n^3 \bar{\nu} \cdot V^2 \Delta\mu^2 \qquad (10)$$

where h, c, and n were defined above, and $\bar{\nu}$ is the energy of the CT emission in wavenumbers. This expression assumes a two-state model for relating the transition moment for the radiative recombination to the change in state dipole moment.[62] If a locally excited state is close in energy to the CT state, interaction with this state requires the use of a three-state model to accurately relate k_r to V.[63] The values of k_r for radiative recombination of $\mathbf{An}^+$-$\mathbf{ANI}^-$ and $\mathbf{MeOAn}^+$-$\mathbf{ANI}^-$ were determined from the emission quantum yields, φ, and lifetimes, τ, of these states given in Table 4 using the relation $k_r = \varphi/\tau$. The values of k_r are 9.6×10^7 and 6.6×10^6 s^{-1}, respectively. The transient absorption data for **An-ANI** and **MeOAn-ANI** in toluene show that the quantum yield for charge separation in each case is > 99%. Thus, we can estimate the value of $\Delta\mu$ by using the charge separation distance of 7.7 Å × 4.8 D/Å =

(61) Smirnov, S. N.; Braun, C. L.; Greenfield, S. R.; Svec, W. A.; Wasielewski, M. R. *J. Phys. Chem.* **1996**, in press.
(62) Marcus, R. A. *J. Phys. Chem.* **1989**, *93*, 3078−3086.
(63) Bixon, M.; Jortner, J.; Verhoeven, J. W. *J. Am. Chem. Soc.* **1994**, *116*, 7349−7355.

37 D. This agrees very well with the 35 D dipole moment for **MeOAn$^+$-ANI$^-$-NI** obtained recently from transient conductivity experiments.[61] Neglecting the ground state dipole moment, eq 10 yields $V = 1850$ and 510 cm^{-1} for the charge recombination reactions in **An$^+$-ANI$^-$** and **MeOAn$^+$-ANI$^-$**, respectively. Due to the proximity of the energy of **An$^+$-ANI$^-$** to that of **^{1*}ANI**, the value of V determined for **An$^+$-ANI$^-$** using the two-state model may be open to question.

We can use these values of V, the solvent reorganization energy of toluene calculated from eq 4 using $r_1 = r_2 = 3.5$ Å and $r_{12} = 7.7$ Å to give $\lambda_s = 0.06$, and the internal reorganization energy of about $\lambda_i = 0.3$ to predict the rate of charge recombination using eq 11, the standard expression from semiclassical electron transfer theory[64−66]

$$k_{CT} = \frac{V_{DA}^2}{\hbar}\sqrt{\pi/\lambda_s k_B T}\sum_{j=0}^{\infty}\exp(-S)\frac{S^j}{j!}\exp\left(-\frac{(\Delta G + \lambda_s + j\hbar\omega)^2}{4\lambda_s k_B T}\right) \quad (11)$$

where ω is the vibrational quantum, usually assumed to be 1500 cm^{-1} and $S = \lambda_i/\hbar\omega$. The summation j is done over the quantum number of the high frequency vibrational modes in the radical pair state. The values of ΔG are taken from those in Table 3. Equation 11 predicts rate constants of 6.0×10^6 and 6.5×10^6 s^{-1} for the charge recombination reaction of **An$^+$-ANI$^-$** and **MeOAn$^+$-ANI$^-$**, respectively. These values are approximately a factor of 30 smaller than the actual rate constants for charge recombination. Of all the terms within eq 11 the values of λ_s and λ_i are most subject to uncertainty. Increasing λ_i by only 0.1 eV or increasing λ_s by only 0.2 eV in eq 11 yields calculated rate constants that agree with the experimental rate constants for these reactions. Thus, it is likely that the discrepancy in the rate constants calculated using eq 11 and those measured experimentally are most likely due to a small increase in the total reorganization energy for the charge recombination process over that calculated from the simple theoretical expressions such as eq 4. In addition, toluene may be acting like a somewhat more polar solvent than suggested by its static dielectric constant. This is supported by the known multipolar nature of the charge distribution within toluene.

Conclusion

We have demonstrated that rod-like triads that consist of a chromophore that possesses a CT excited state and aromatic diimide acceptors are capable of generating long-lived giant dipole states in high yield. Triad **MeOAn-ANI-NI** in toluene generates a fully charge-separated state with a quantum yield of 0.92 that stores ∼2 eV for over 300 ns. The unambiguous spectral characterization of all of the electronic states involved in the charge transfer sequence is without precedent. The emissive nature of the intermediate ion pair states allows us to analyze the role of CT states in affecting electron transfer rates. The primary charge separation step can be considered formation of the CT excited state of the ANI chromophore followed by two charge shift reactions that rapidly separate the charges. The rapid forward electron transfer rate of the first electron transfer step combined with the slow rate of charge recombination from the initial ion pair state makes this series a powerful platform for studying the details of subsequent charge shift reactions. Further work in this area is in progress.

(64) Hopfield, J. J. *Proc. Natl. Acad. Sci. U.S.A.* **1974**, *71*, 3640−3644.
(65) Jortner, J. *J. Chem. Phys.* **1976**, *64*, 4860−4867.
(66) Marcus, R. A. *J. Chem. Phys.* **1984**, *81*, 4494−4500.
(67) Gosztola, D.; Yamada, H.; Wasielewski, M. R. *J. Am. Chem. Soc.* **1995**, *117*, 2041−2048.

Experimental Section

All solvents were HPLC grade. Details concerning the synthesis and spectroscopic characterization of the molecules employed in this study are given in the supporting information.

Transient absorption data was taken with a pump wavelength of either 412 or 420 nm. The laser system used for the transient absorption experiments was a regeneratively-amplified Ti:sapphire laser that has been described before.[67] This description and the following summary describe the current laser system used to generate 412 nm excitation pulses with major differences for the 420 nm pump system shown in parentheses. Briefly, the ∼50-fs (150-fs at 420 nm) output of a Ti:sapphire oscillator operating at 824 nm (840 nm for 420-nm pump) was stretched to a few hundred picoseconds and used to seed a Ti:sapphire regenerative amplifier. The amplifier was pumped by an intracavity-doubled Q-switched Nd:YAG laser operating at 1.3 kHz. The output of the amplifier was recompressed in a two-grating compressor to ∼140 fs (∼250 fs at 420 nm), with typical energies of 200 μJ after compression. The recompressed pulse was beamsplit 9:1, with the more intense beam doubled in a 2-mm thick Type I LBO crystal ($\phi = 28°$, $\theta = 90°$), providing 70-μJ pulses at 412 nm. The weaker beam was focused with an $f_0 = 200$ mm lens into a 6-mm-thick fused silica block rotating at 2 RPD to avoid damage. A stable white light continuum was generated by carefully adjusting the intensity of the 824-nm pump with a waveplate-polarizer pair to slightly above threshold. Continuum intensity fluctuations were typically under 5%. The white light was dechirped with a double-passed grating pair. The white light beam was beamsplit into a probe and reference beam.

The 412-nm pump beam was sent down a computer-controlled 1.3-m delay line. Delays of 6 ns were possible with 6.6 fs resolution. The pump and probe beams were focused at the sample with separate 750- and 400-mm lenses at a shallow angle, producing spot sizes (diameter) of 400 and 300 μm, respectively. The pump energy was attenuated with a waveplate-polarizer pair, and typical energies were 2−5 μJ. The polarizer sets the pump at 45° with respect to the probe. The probe and reference beams were set to be vertically displaced with respect to each other and were focused into a computer-controlled monochromator (Spex 270M) with a 75-mm lens. The beams were spatially separated after the exit slit, and the probe beam was separated into parallel and perpendicular components with a calcite polarizer. The three beams were detected with matched silicon photodiodes operated in photovoltaic mode and amplified with transimpedence amplifiers. The amplifier outputs were measured by gated integrators and digitized with a 12-bit A/D board, thus providing simultaneous acquisition of the parallel and perpendicular components of the data. (For the 420-nm pump data, the pump and probe beams were set at the magic angle and detected directly after the monochromator with a pair of photodiodes.)

A mechanical chopper was inserted in the pump beam and synchronized to one half of the laser repetition rate, resulting in every other pump pulse being blocked. Each shot pair (pump on, pump off), resulted in a single ΔA measurement. The reference pulse, in addition to being used for the ΔA calculation, was also used to discriminate against probe pulses of abnormal intensity. Typically, measurements were accepted only when the reference was within ±10% of the center value, which usually results in less than 10% of the shots being rejected. Of course, the discrimination was possible only with kinetic decays, as the intensity of the white light varies substantially with wavelength. Data sets were typically the average of roughly ten scans, with each point in the scan being the average of one hundred laser shots. All reported kinetics are isotropic, calculated from the parallel and perpendicular data sets (iso. $= (\| + 2\perp)/3$) (with the 420-nm pump, magic angle detection directly gives isotropic kinetics). Kinetic parameters were determined using a grid-search fitting algorithm.

Samples for the transient absorption experiments had optical densities for 1-cm pathlength cells of ∼0.5 (concentration $< 10^{-4}$ M), except in the case of **MeOAn-ANI-NI**, which was limited to an OD of ∼0.25 by its solubility. Samples were stirred during the experiment to prevent thermal lensing.

Microsecond experiments were performed with a 10-Hz Nd:YAG laser system. The 416-nm pump was created by Raman shifting (with

a 700-PSI H_2 pressure cell) the 355-nm, third harmonic output of the laser. The probe light was generated by a xenon flashlamp (EG&G Electro-Optics FX-200) and detected by a photomuliplier tube (Hamamatsu R928). Traces were time-resolved with a Tectronix 7912 Transient Digitizer and averaged by computer. Degassed samples were prepared by several freeze−pump−thaw cycles, and low concentrations (concentration $\sim 5 \times 10^{-6}$ M, OD ~ 0.03) were used on the half-millisecond scans to avoid artifacts due to triplet-triplet annihilation.

Absorption measurements were made on a Shimadzu spectrometer (UV160). Fluorescence measurements were made on a single-photon-counting fluorimeter (PTI). Sample absorption to the red of the excitation wavelength was kept below 0.1 to avoid reabsorption artifacts. A solution of fluorescein in 0.1 M NaOH was used as the standard for quantum yield measurements ($\phi = 0.90$).

Acknowledgment. This work was supported by the Division of Chemical Sciences, Office of Basic Energy Sciences of the United States Department of Energy under contract W-31-109-Eng-38. S.R.G. would like to acknowledge an appointment to the Distinguished Postdoctoral Research Program sponsored by the U.S. DOE, Office of Science Education and Technical Information.

Supporting Information Available: Synthesis and spectroscopic characterization of the molecules employed in this study (10 pages). See any current masthead page for ordering and Internet access instructions.

JA9600789